Synthesis of Nitrogen-Doped Porous Carbon Nanofibers as an Efficient Electrode Material for Supercapacitors

Li-Feng Chen,[†] Xu-Dong Zhang,[†] Hai-Wei Liang,[†] Mingguang Kong,[‡] Qing-Fang Guan,[†] Ping Chen,[†] Zhen-Yu Wu,[†] and Shu-Hong Yu[†,‡,*]

[†]Division of Nanomaterials & Chemistry, Hefei National Laboratory for Physical Sciences at Microscale, Department of Chemistry, Department of Materials Science & Engineering, the National Synchrotron Radiation Laboratory, University of Science and Technology of China, Hefei 230026, People's Republic of China and [‡]Key Laboratory of Materials Physics, Institute of Solid State Physics, Chinese Academy of Sciences, Hefei, 230031, People's Republic of China

ABSTRACT

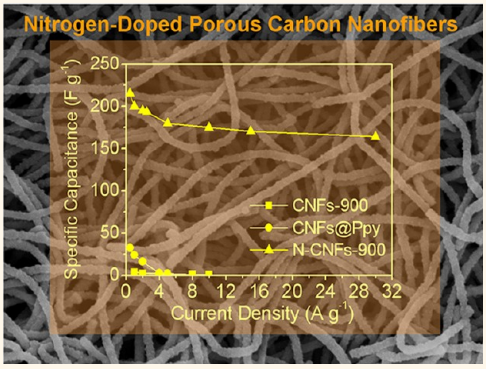

Supercapacitors (also known as ultracapacitors) are considered to be the most promising approach to meet the pressing requirements of energy storage. Supercapacitive electrode materials, which are closely related to the high-efficiency storage of energy, have provoked more interest. Herein, we present a high-capacity supercapacitor material based on the nitrogen-doped porous carbon nanofibers synthesized by carbonization of macroscopic-scale carbonaceous nanofibers (CNFs) coated with polypyrrole (CNFs@polypyrrole) at an appropriate temperature. The composite nanofibers exhibit a reversible specific capacitance of 202.0 F g^{-1} at the current density of 1.0 A g^{-1} in 6.0 mol L^{-1} aqueous KOH electrolyte, meanwhile maintaining a high-class capacitance retention capability and a maximum power density of 89.57 kW kg^{-1}. This kind of nitrogen-doped carbon nanofiber represents an alternative promising candidate for an efficient electrode material for supercapacitors.

KEYWORDS: nitrogen-doped porous carbon nanofibers · scale-up production · electrode material · supercapacitors

With close attention paid to the world ecology and economy, people are observing the bountiful, low-cost, and clean energy from sun and wind which, in principle, should be able to satisfy the ever increasing and urgent demand. However, most of the renewable energy is intermittent and cannot meet the needs for casual use, except for converting to electricity.[1,2] Supercapacitors offer a most promising approach for fast storing the excess electrical energy.[3,4] In addition, supercapacitors are required in other areas, such as portable electronics, hybrid electric vehicles, and stand-by power systems.[2,5−7] As a new type of energy storage devices, the supercapacitors are different from traditional capacitors, which combine the advantages of both conventional dielectric capacitors and rechargeable batteries and can transport high power within a very short period and store high energy.[8]

The performance of these devices depends intimately on the physical and chemical properties of their electrode materials.[3] Therefore, it is urgent to develop excellent electrode materials. Early in 1990, the development of electrochemical capacitors for high-power applications started when researchers recognized the potential of using high surface area carbons to achieve the devices.[9] Since then, some carbon materials, such as activated carbon,[7] carbon black,[10] carbon onions,[10,11] carbon nanotubes,[12,13] and graphene, have been the most commonly employed for electrode materials to improve the capacity.[14] Although most of the porous materials exhibit large capacitances, the electrical conductivity suffers from a decrease with increasing porosity due to noncompatibility of conductive pathways or oxygen-containing functional groups,[15,16] which largely limits the power capacity. Thus, this calls for the development of carbon materials with high surface area, energy density, and specific conductivity properties (to improve the power density). Of course, the long cycle life is a key development parameter.[8]

To further enhance the energy density and specific power of capacitors, the strategy of utilizing electrode materials possessing

* Address correspondence to shyu@ustc.edu.cn.

Received for review May 15, 2012 and accepted July 7, 2012.

Published online July 07, 2012
10.1021/nn302147s

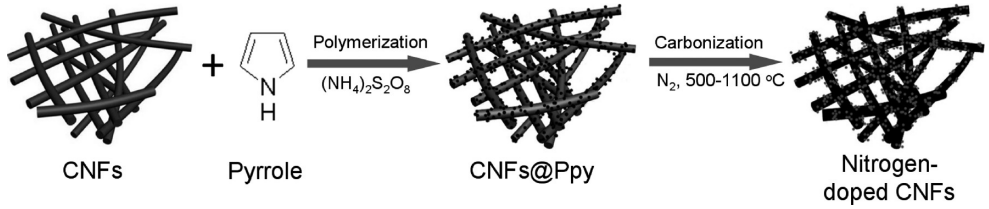

Scheme 1. Schematic illustration for the fabrication processes of nitrogen-doped CNFs.

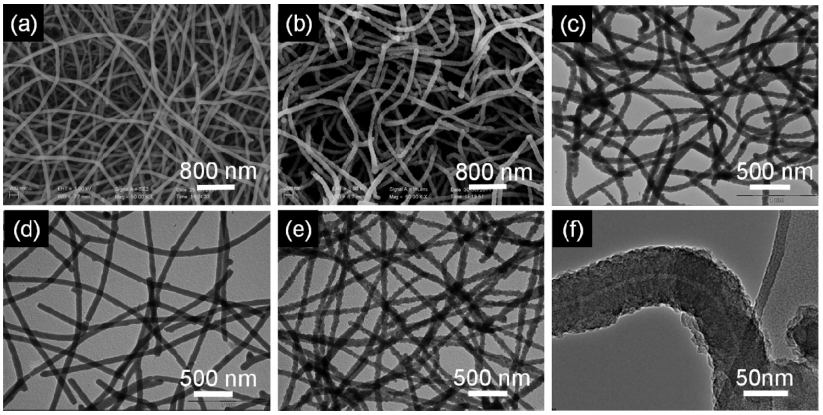

Figure 1. (a,b) High-resolution FE-SEM images of CNFs and CNFs@Ppy. (c) Low-resolution TEM images of N-CNFs-900. (d–f) High-resolution TEM images of CNFs, CNFs@Ppy, and N-CNFs-900.

pseudocapacitance properties is a vital candidate. In this respect, one approach is to introduce heteroatoms into carbon frameworks.[16–23] It has been reported that certain nitrogen doping seems to be the most promising method for enhancing capacity,[16,24] surface wettability of the materials,[25] and electronic conductivity[26] while maintaining the superb cycle ability.[27] In most cases, plenty of nitrogen-doped carbon materials have been achieved by introducing nitrogen onto carbon frameworks through the post-treatment, for example, treating it with ammonia gas/air,[28–30] which results in a lower content of nitrogen. The drawback can be overcome by employing N-containing materials as precursors.[31–35] By this method, nitrogen can be preserved at a relatively large content by adjusting the carbonization temperature. Meanwhile, the preparation procedure is simple, and the nitrogen on the carbon framework can stay stable under a harsh working condition. However, to date, by that means it often uses expensive sacrificed scaffolds (mesoporous silica or zeolites) for nanocasting routes (which involve harsh experimental conditions or costly synthetic processes)[35,36] or undergoes a direct carbonization of the nitrogen-enriched precursor with a time-consuming activation.[31,33,37] Thus, the relatively easily produced nitrogen-doped carbon materials with proper porosity and good electrical conductivity are highly desirable.

Recently, we have developed a simple template-directed hydrothermal carbonization (HTC) process for controlled synthesis of carbonaceous nanofibers (CNFs) and monolithic hydrogels/aerogels on macroscopic scale (12 L).[38–40] In this work, we present a facile route to prepare the high-content nitrogen-doped porous CNFs containing graphitic frameworks by using our macroscopic-scale CNFs as the precursor. More importantly, the results have demonstrated that nitrogen-doped porous carbon nanofibers exhibit great potential as an efficient electrode material for supercapacitors with favorable electrochemical performance, that is, a relatively high specific capacity and excellent rate performance when compared with the most popular N-containing carbon materials, as well as cycling stability. Furthermore, all of the precursors used in the process can be synthesized on large-scale or are commercially available, which will be suitable for scale-up production.

RESULTS AND DISCUSSION

A schematic illustration for the preparation of nitrogen-doped carbonaceous nanofibers is presented in Scheme 1. The CNFs@polypyrrole (CNFs@Ppy) was synthesized *via* the CNF template first and then carbonized under N_2 for 2 h. Our recent studies demonstrated that the carbonaceous nanofibers can be fabricated on a macroscopic scale by a simple hydrothermal carbonization process.[40] In this work, we use the typical CNFs of 70 nm in diameter as the template to synthesize representative precursor CNFs@Ppy on large scale, which is quite facile without the need of expensive apparatus or the assistance of heating or cooling. We found that the surfaces of the CNFs were very smooth (Figure 1a,d and Supporting Information Figure S1a), while all of the CNFs@Ppy with a diameter

of about 85 nm showed comparatively rough surfaces (Figure 1b,e and Supporting Information Figure S1b). The minor difference of the surface morphology between CNFs and CNFs@Ppy suggested that the surfaces of CNFs were coated by Ppy quite well. After that, the CNFs@Ppy was carbonized in N_2 atmosphere, resulting in the formation of nitrogen-doped CNFs.

Previously, it has been found that the carbonization temperature plays a crucial role in the synthesis process.[33,35] In the case of nitrogen-doped CNFs, nitrogen species, nitrogen contents, and pore structures strongly depend on the carbonization temperature of the CNFs@Ppy precursor. Nevertheless, the synthesis of the carbon nanofiber materials with a relatively large amount of a certain type of nitrogen and, at the same time, appropriate porous texture is not an easy task since there is an unavoidable detriment in the nitrogen functionalities.[8,29,36] Hence, it is necessary to optimize the carbonization process. Herein, the precursor CNFs@Ppy was annealed at 500, 700, 900, and 1100 °C in N_2 atmosphere at a flow rate of 150 cm^3 min^{-1} (denoted as N-CNFs-500, N-CNFs-700, N-CNFs-900, and N-CNFs-1100, respectively). The effect of the reaction temperature on the pore evolution, nitrogen content, and species of the resulting materials as well as the supercapacitor performance was analyzed in detail. The TEM images of N-CNFs-500, N-CNFs-700, N-CNFs-900, and N-CNFs-1100 are shown in Figure S2 (Supporting Information) and Figure 1c,f. It can be seen that with the increase of carbonization temperature, the diameter of N-CNFs becomes a little smaller. On the basis of the previous studies,[31] the burnoff and shrinkage of the polypyrrole precursor will be enhanced when the carbonization temperature increases; therefore, the diameter will become smaller. Moreover, the N-CNFs-900 exhibits a large amount of interstitial pores.

The samples were analyzed by powder X-ray diffraction (XRD) in the wide-angle region (Supporting Information Figure S3). From the most relevant characteristic peaks at $2\theta = 21.99$ and 43.56°, it was clear that the N-CNFs consists of graphitized carbon ascribed to the carbonization of the CNFs@Ppys.[6] Particularly, for N-CNFs-900 and N-CNFs-1100, with the increase of carbonization temperature, the intensity of the peak at around 21.99° increased, while the full width at half-maximum decreased. The intensity of the other peak at around 43.56° also rose a little with increasing temperature. These observations suggest that the degree of graphitization becomes higher with the increase of carbonization temperature.[6] In contrast, only one wide diffraction peak was observed for the CNFs@Ppy, which indicates that this material has amorphous nature and does not contain graphitized carbon. The XRD patterns revealed that the CNFs@Ppy contains a poorly organized carbon (turbostratic order) and the N-CNFs is composed of graphitic structures, which can greatly affect their electrical conductivity.[35]

To understand the role of nitrogen functionalities in capacitive performance, it is necessary to clarify the types of nitrogen introduced onto the carbon surface *via* X-ray photoelectron spectroscopy (XPS) (Figure 2). The XPS survey spectra of all of the samples are shown in Figure 2a. The percentage of nitrogen in CNFs@Ppy, N-CNFs-500, N-CNFs-700, N-CNFs-900, and N-CNFs-1100 was calculated from the XPS survey spectrum to be around 12.14, 12.04, 9.57, 7.22, and 4.02%, respectively. The deconvolutions of the N 1s region spectrum to identify the surface functionalities are shown in Figure 2b–f and fitted by three component peaks, which are attributed to three types of nitrogen functional groups, namely pyridinic (N-6), pyrrolic/pyridone (N-5), and quaternary nitrogen (N-Q).[6,16] From Figure 2b, it can be seen that, for CNFs@Ppy, the only peak at 399.7 eV corresponds to N atoms within the pentagonal ring of the polypyrrole (N-5).[33,41] For N-CNFs-500 in Figure 2c, the other two peaks of N-6 (398.0 eV) and N-Q (400.7 eV) appear, and the N-5 peak (399.7 eV) becomes much weaker than that of CNFs@Ppy due to the carbonization. Upon further increasing the carbonization temperature for N-CNFs-700 (Figure 2d), the intensity of the N-5 peak became much weaker and its proportion was obviously smaller than that of N-CNFs-500 and CNFs@Ppy, whereas the peaks of N-6 and N-Q rose largely. At higher carbonization temperatures, the N-5 peak is not observed and only the N-6 and N-Q peaks are found in the case of N-CNFs-900 and N-CNFs-1100 (Figure 2e,f). Additionally, when the carbonization temperature increased, the values of n(N-6)/n(N-Q) [n(N-6)/n(N-Q) values of N-CNFs-500, N-CNFs-700, N-CNFs-900, and N-CNFs-1100 are 31.31, 27.35, 23.13, and 14.36%, respectively] decreased in the N-CNFs, indicating the formed N-Q is much more stable than N-6 at high temperatures.[6] These results demonstrate that N atoms within the pentagonal ring of polypyrrole are progressively converted to two types of nitrogen (N-6 and N-Q) in the carbonization process, as previously found in other materials.[6,33,42] Hence, the carbonization of CNFs@Ppys may be a good method to introduce surface functionalities into the carbon materials. Moreover, the plentiful accessible N-containing species (N-6 and N-Q) would provide chemically active sites to improve the power density of supercapacitors.[43]

For the convenience of comparison with N-CNFs-500, N-CNFs-700, N-CNFs-900, and N-CNFs-1100, the CNFs were also annealed in the same condition to obtain CNFs-900. Figure 3a shows the N_2 adsorption–desorption isotherms of the samples. For the CNFs@Ppy, it shows an intermediate shape between types II and IV (in the IUPAC classification) with a small hysteresis loop extending from $P/P_0 = 0.80$ to *ca.* 0.99.[44] After the carbonization reaction, CNFs-900, N-CNFs-500, N-CNFs-700, N-CNFs-900, and N-CNFs-1100 exhibited N_2

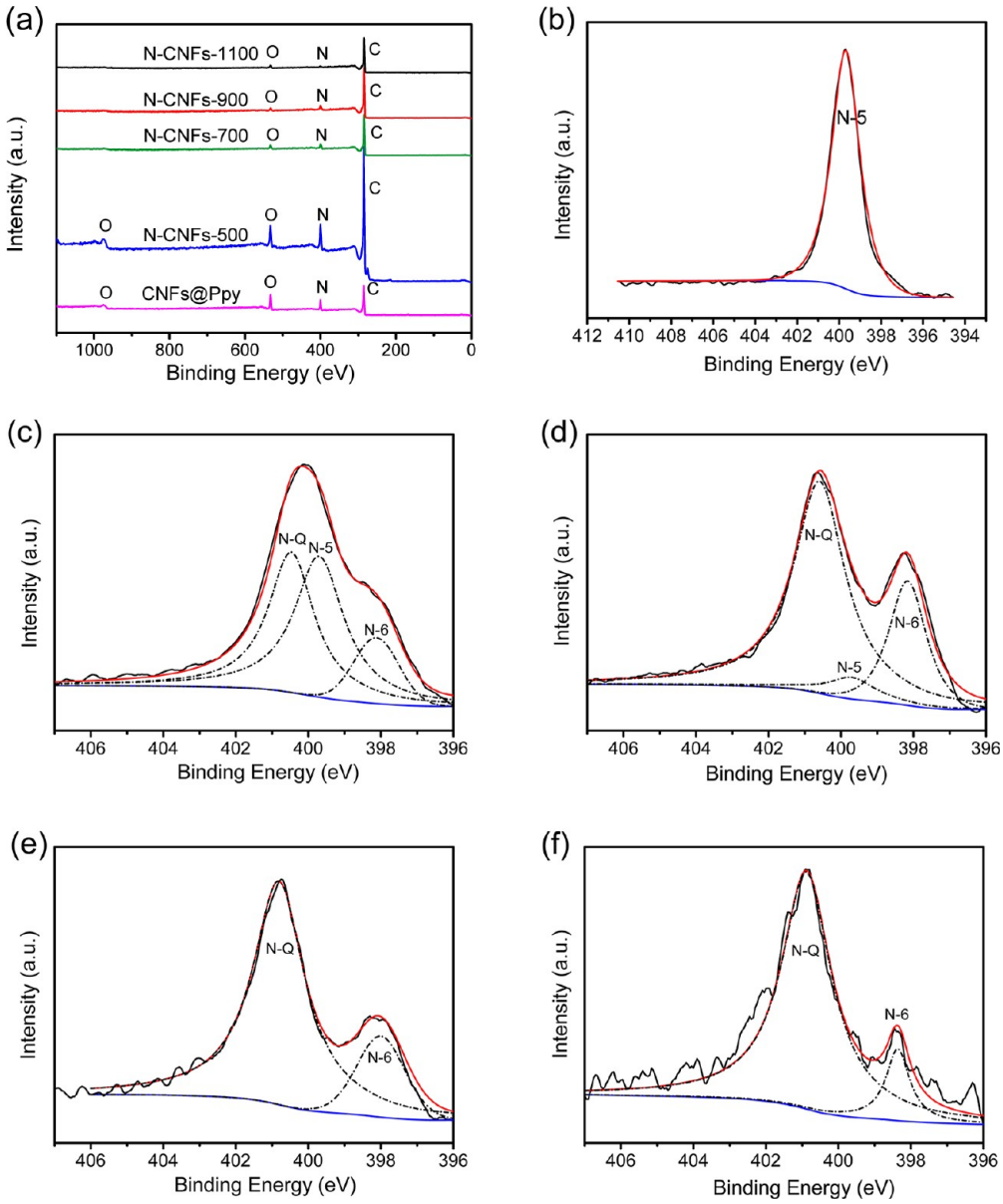

Figure 2. (a) XPS survey spectra of CNFs@Ppy and N-CNFs. (b−f) High-resolution XPS spectra of the deconvoluted N 1s peak: (b) CNFs@Ppy, (c) N-CNFs-500, (d) N-CNFs-700, (e) N-CNFs-900, and (f) N-CNFs-1100.

isotherms close to type IV with steep uptakes below $P/P_0 = 0.01$ and clear hysteresis loops, which indicated the coexistence of micropores (<2 nm) and mesopores (2−50 nm) in these samples.[45] The porous properties of these materials are summarized in Table 1, including the specific surface area (S_{BET}), total pore volume, and average pore diameter. It can be seen that the S_{BET} increases from 293.63 to 562.51 $m^2\ g^{-1}$ during the annealed temperature of 500−900 °C but falls slowly to 524.09 $m^2\ g^{-1}$ at 1100 °C, and the average pore diameter of N-CNFs-900 becomes obviously smaller than that of CNFs@Ppy and other N-CNFs probably owing to the emission of many non-carbon or carbon elements and enhancement of the burnoff of CNFs@Ppy when the carbonization temperature increases.[31]

The pore size distribution (PSD) curves give a wealth of information regarding the distribution of different size pores. Here, we performed the measurement in the range of 0.5−100 nm (Figure 3b) and analyzed it. To better understand the pore distribution of the materials, we magnified the 0.5−5 nm region (inset in Figure 3b) and surprisingly found that the carbonization temperature also plays a critical role in controlling the pore structure of the resulting samples. The N-CNFs-900 not only had sharp peaks at ~0.50, 0.64, 1.18, 2.52, and 9.32 nm but also had slightly sharp ones at 25.24 and 68.54 nm, indicating the coexistence of hierarchical micropores, mesopores, or macropores in the N-CNFs-900. In comparison, CNFs-900, CNFs@Ppy, N-CNFs-500, N-CNFs-700, or N-CNFs-1100 contains relatively less micropores, mesopores, or macropores.

From the above discussion, we can conclude that the carbonization at the temperature of 900 °C made the CNFs@Ppy turn into the porous nitrogen functionalized carbon nanofiber (N-CNFs-900) with a large specific surface area, localized graphitic structure, and interconnected pores (for one clear H3-type hysteresis loop from $P/P_0 = 0.12-0.99$ in the nitrogen isotherms) which seems to be composed of micropores, mesopores (some mesopores are derived from the intercrossed stack of nanofibers), or macropores, and a template method in the synthesis of N-CNFs offers an effective way to produce well-controlled nitrogen-doped nanofibers. Hence, there has been great progress in the synthesis of nitrogen-doped porous texture carbon nanofibers through our template technique making the N-CNFs-900 a possible promising candidate for electrode materials of supercapacitors.

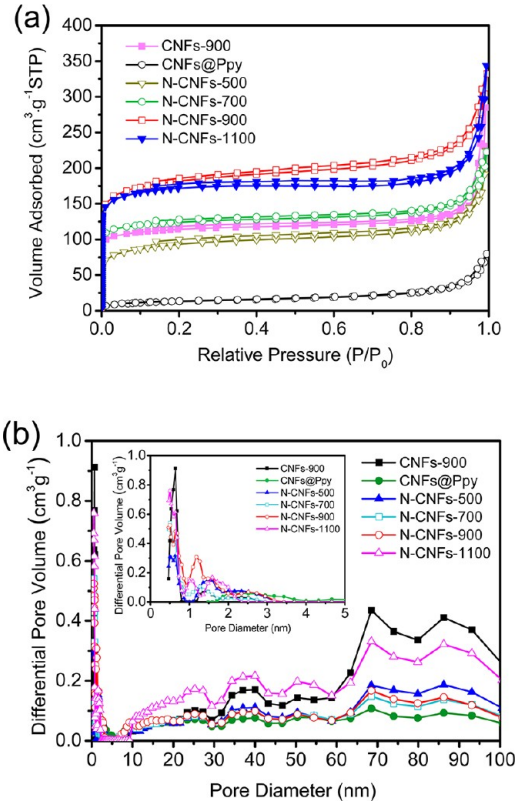

Figure 3. (a) Nitrogen adsorption−desorption isotherms and (b) pore size distribution (inset: magnified 0−5 nm region) of CNFs-900, CNFs@Ppy, N-CNFs-500, N-CNFs-700, N-CNFs-900, and N-CNFs-1100.

It is expected that the N-CNFs-900 will have impressive electrochemical performance, and further characterizations have been carried out to prove this hypothesis. To the best of our knowledge, the majority of reports on electrodes composed of N-enriched carbon materials provide the capacitance values with a three-electrode system.[27] For the sake of consistency and comparability, the capacitance value and cycling performance of our samples were studied in 6 mol L^{-1} aqueous KOH using three-electrode cells at room temperature.

To evaluate the properties of the porous nitrogen-doped carbon nanofibers as supercapacitor electrodes, we first carried out cyclic voltammetry (CV) measurements at different potential sweep rates (Figure 4a-d and Figure 5a). From the CV curves shown in Figure 4a, the remarkable difference in electrochemical surface activity between the CNFs-900, CNFs@Ppy, and the N-CNFs can be easily recognized. In detail, the CNFs-900 and CNFs@Ppy exhibited small rectangular curves corresponding to low capacitances due to no heteroatom or very low S_{BET}, while the N-CNFs presents capacitive behavior with the appearances of roughly rectangular-like shapes and a few humps in these CV curves owing to the combination effects of electric double-layer capacitance (EDLC) and pseudocapacitance.[46] We also observed that the N-CNFs-900 still kept the "rectangular shape" cyclic voltammogram even at a potential scan rate of 200 mV s^{-1} (Figures 4d and 5a). In contrast, the CV curves of other samples were obviously distorted with increasing the scan rate from 5 to 100 mV s^{-1} mainly due to the limited ion incorporation into the active electrode material (Figure 4a−c). In addition, it follows from the voltammetry characteristics that N-CNFs-900 possesses a good capacitor response and low equivalent series resistance (ESR).

In order to further investigate the performance of our samples, galvanostatic charge/discharge experiments were performed at various current densities in a three-electrode system with the voltage windows the same as that for the above CV analysis. As shown in the galvanostatic charge/discharge curves (Supporting Information Figure S4a,b), the discharging time of the N-CNFs-900 was significantly longer compared with that of other materials at both high and low current densities, indicating that the N-CNFs-900 offers a much larger capacitor, which agrees well with those obtained from CV tests. Moreover, the galvanostatic charge/discharge curve of N-CNFs-900 is nearly symmetric with a gradual

TABLE 1. Physicochemical Characterization of CNFs-900, CNFs@Ppy, N-CNFs-500, N-CNFs-700, N-CNFs-900, and N-CNFs-1100 Nanocomposite

item	CNFs-900	CNFs@Ppy	N-CNFs-500	N-CNFs-700	N-CNFs-900	N-CNFs-1100
BET surface area (m^2 g^{-1})	348.12	46.75	293.63	378.68	562.51	524.09
t-method external surface area (m^2 g^{-1})	74.14	41.04	119.98	76.54	165.04	105.45
total pore volume (cm^3 g^{-1})	0.44	0.078	0.35	0.34	0.51	0.53
average pore diameter (nm)	5.07	6.66	4.73	3.65	3.64	4.06

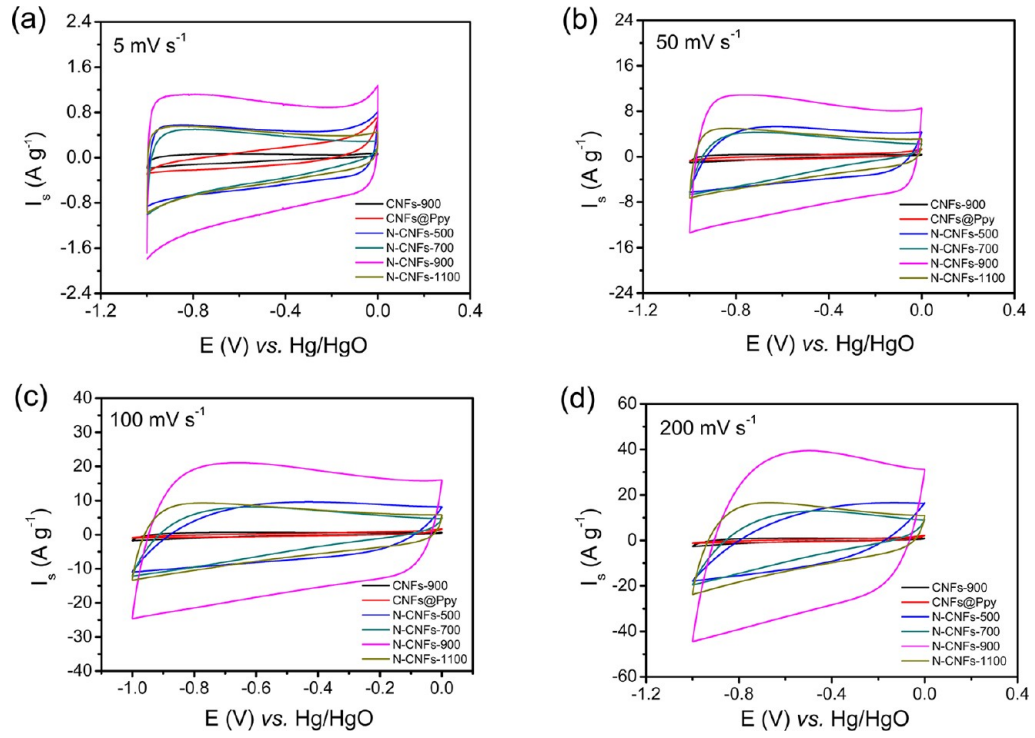

Figure 4. Cyclic voltammograms of CNFs-900, CNFs@Ppy, N-CNFs-500, N-CNFs-700, N-CNFs-900, and N-CNFs-1100 at a scan rate of (a) 5 mV s $^{-1}$, (b) 50 mV s $^{-1}$ (c) 100 mV s $^{-1}$, and (d) 200 mV s $^{-1}$.

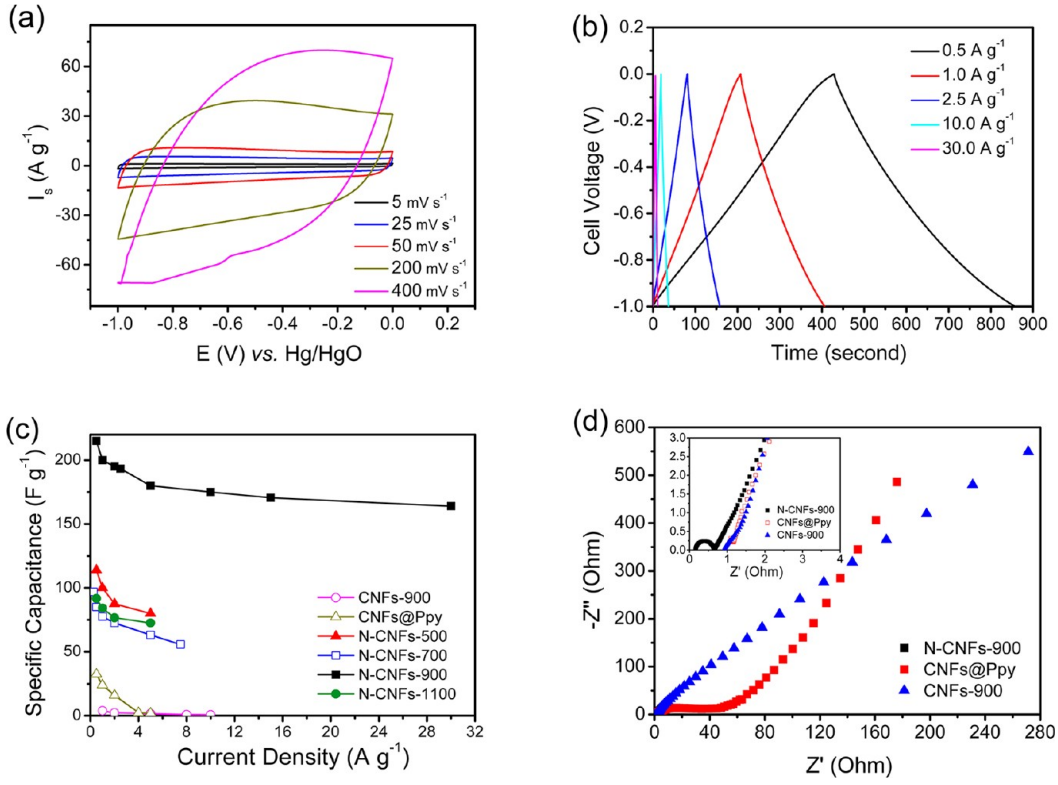

Figure 5. Electrochemical performances measured in a three-electrode system. (a) Cyclic voltammograms of N-CNFs-900 at different scan rates and (b) charge−discharge curves of N-CNFs-900 at different current densities. (c) Specific capacitances of CNFs-900, CNFs@Ppy, N-CNFs-500, N-CNFs-700, N-CNFs-900, and N-CNFs-1100 at different current densities. (d) Electrochemical impedance spectra (inset: magnified 0−4 Ω region) under the influence of an ac voltage of 5 mV.

slope change (Figure 5b and Supporting Information Figure S4b). On the contrary, the galvanostatic charge/discharge curves of other samples are not very symmetric or bent. Additionally, for the galvanostatic charge/discharge

at a high current load of 5.0 A g^{-1}, the Ohmic drop of the N-CNFs-900 is rather limited compared with other samples, which is attributed to the existence of the appropriate quantity of mesopores in the sample (which speeds up the rate of ion transfer and maybe reduce the inner resistance of the electrodes) and its good conductivity (which can be further confirmed by the electrochemical impedance spectroscopy measurements).[46]

It is considered that the galvanostatic charge/discharge measurement is a more accurate technique especially for pseudocapacitances.[8] Therefore, the specific capacitances in the present case were calculated from galvanostatic charge/discharge curves according to the following equation:[8,47]

$$C_s = \frac{I \times \Delta t}{m \times \Delta V} \quad (1)$$

where C_s (F g^{-1}) is the specific capacitance, I (A) refers to the discharge current, ΔV (V) represents the potential change within the discharge time Δt (s), and m (g) corresponds to the amount of active material on the electrode. It is found that the electrode material N-CNFs-900 possessed a substantially higher specific capacitance than CNFs@Ppy, CNFs-900, and other N-CNFs. That is, at 1.0 A g^{-1}, the specific capacitance for the N-CNFs-900 electrode is 202.0 F g^{-1}, which is more than twice that of the N-CNFs-500 electrode (99.4 F g^{-1} at 1.0 A g^{-1}) and much higher in comparison with the CNFs-900, CNFs@Ppy, N-CNFs-700, and N-CNFs-1100. Moreover, we compared our results with major published data on N-enriched carbon materials (Table 2) and listed the major characteristics of each report, such as the origin, used electrolytes, and the normalized capacitances. Clearly, our C_s value of the N-CNFs-900 is much higher than that of most of the nitrogen-containing carbon materials. With referrence to the previous reports,[6,8,24,36,46] the sample N-CNFs-900 of high specific capacitance may be attributed to the combined effect of a high nitrogen doping level changing the electron donor/acceptor characteristics of carbon and a large BET surface area increasing the surface area accessibility for electrolyte ion transport.[6]

Besides, it is well-known that an ideal supercapacitor should be able to deliver the same energy under any operation conditions. As a result, it is important to investigate the capacitance retention at a higher current density.[10,27] The relationships between C_s value and charge/discharge current density measured in a three-electrode system are presented in Figure 5c. A slight decrease in the C_s of N-CNFs-900 is observed as the current densities go from 0.5 to 1.0 A g^{-1}, but C_s is maintained quite well under higher current densities (Figure 5c), indicating this electrode material exhibits a good capacitance retention capability, for example, at 30.0 A g^{-1} reaching 164.5 F g^{-1}, which is ~81.72% of the value at 1.0 A g^{-1}. It also reflects that the specific capacitance of the N-CNFs-900 was not kinetically limited.[51] The excellent retention capability, indication of high power density, probably owing to the suitable size distribution of meso/micropores granting effective accessibility for electrolyte even at a higher speed,[47] makes the material directly suitable for application.

TABLE 2. Comparison of the C_s of Some N-Enriched Carbon Materials in the Literature

item	electrolyte	C_s (F g^{-1})	ref
N-rich composite of CNTs and carbon derived from melamine	1 M H_2SO_4	167.0	37
ammoxidized coals	7 M KOH	145.0	29
templated mesoporous N-enriched carbon materials	1 M H_2SO_4	201.0	48
N-enriched carbon from silk fibroins	1 M $TEABF_4$/PC	52.0	49
CNTs/N-enriched carbon	1 M H_2SO_4	100.0	50
N-enriched carbon from melamine—mica	6 M KOH	198.0	27
nitrogen-doped porous nanofibers	6 M KOH	202.0	this work

Electrochemical impedance spectroscopy (EIS) is a powerful measurement that gives a lot of information regarding internal resistance of the electrode material and resistance between the electrode and electrolyte. A Nyquist impedance spectrum of the N-CNFs-900 electrode recorded in a three-electrode system at the open circuit voltage is presented in Figure 5d.[52] Obviously, a small semicircle is observed at the high-frequency region. It is well accepted that a semicircle reflects the electrochemical reaction impedance of the electrode, and a smaller semicircle means smaller charge transfer resistance.[51] On the basis of this point, it is apparent that the solution resistance for the N-CNFs-900 is very low, about 0.14 Ω (1.25 Ω for the CNFs@Ppy and 0.92 Ω for the CNFs-900). The very low ESR is crucial for enhancing rate capability or the power density of the electrochemical capacitors.[51]

Furthermore, we studied the durability of the N-CNFs-900 electrode using galvanostatic charge/discharge measurement to characterize the long-term charge/discharge behavior at a current density of 1.0 A g^{-1}. The specific capacitance of N-CNFs-900 as a function of cycle number, within a potential window of −1.0−0 V *vs* Hg/HgO, is shown in Figure 6a. It is clear that the specific capacitance still remains at about 195.9 F g^{-1} (above 97% of the initial capacitance) after 3000 cycles, which illustrates that the N-CNFs-900 electrode displays a good cycling and stability behavior as the supercapacitive electrode material. Additionally, the triangular shape of the 3000th galvanostatic charge/discharge cycle, shown in Figure 6b, also indicates that the electrode possesses stable performance and good charge propagation.[53]

In order to completely determine the electrochemical performance of our materials, energy density and power density of the electrochemical N-CNFs-900// N-CNFs-900 capacitor were estimated, using the following equations:[54−57]

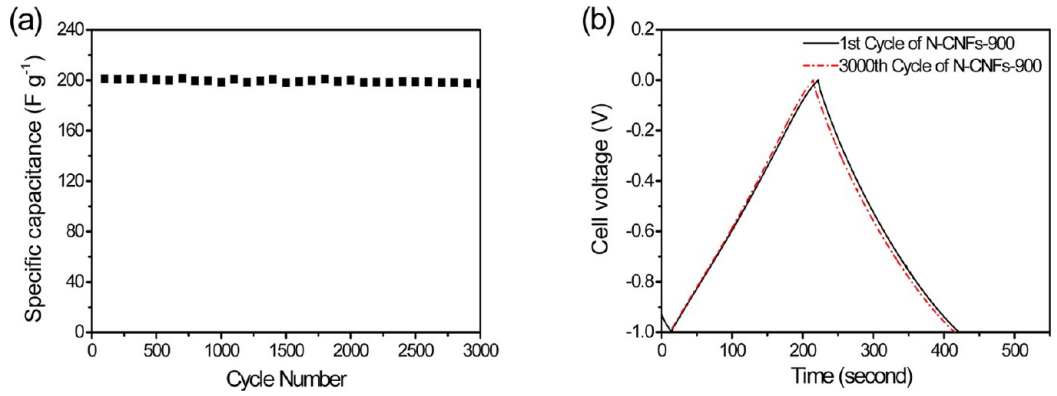

Figure 6. Cycling performance of the N-CNFs-900. (a) Gravimetric capacitance calculated from the discharge curves of 3000 cycles. (b) Triangular shapes of the first and 3000th cycle.

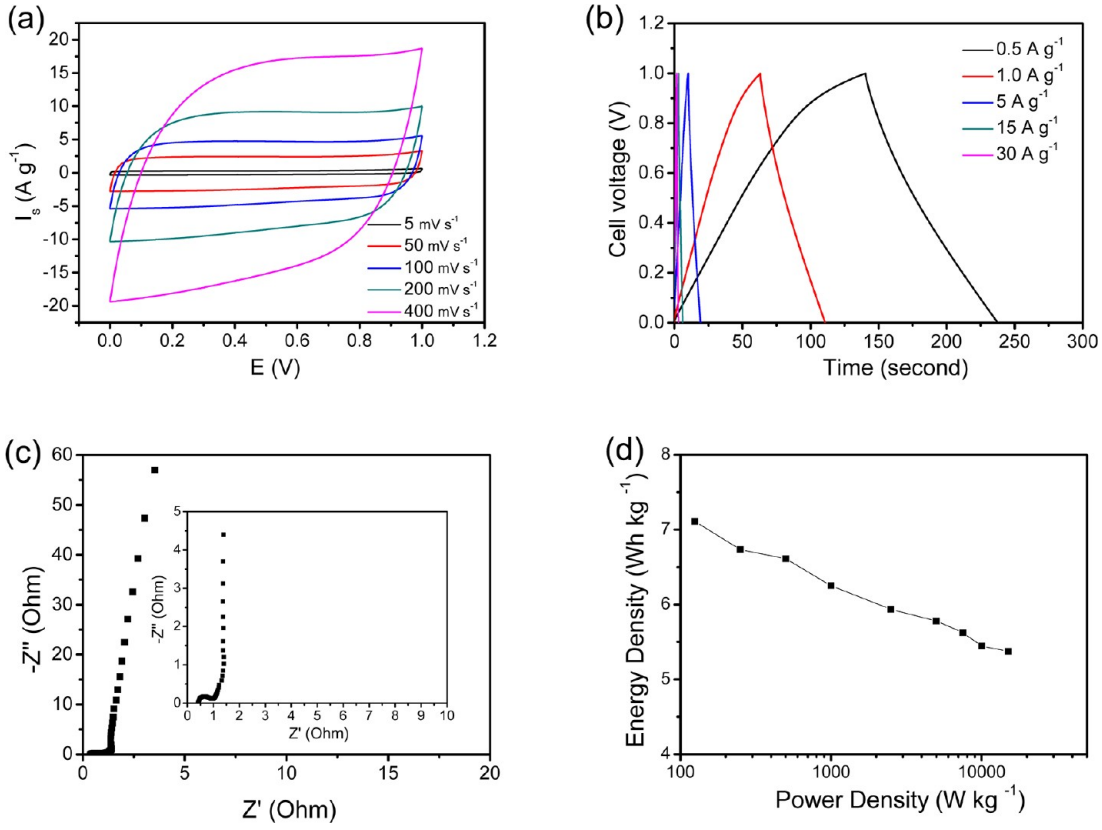

Figure 7. Electrochemical performances of the N-CNFs-900//N-CNFs-900 device measured in a two-electrode system. (a) Cyclic voltammograms at different scan rates. (b) Charge−discharge curves at different current densities. (c) Electrochemical impedance spectra (inset: magnified region) collected under the influence of an ac voltage of 5 mV. (d) Ragone plot performed in 6.0 mol L^{-1} of KOH aqueous solution.

$$C_m = \frac{I \times \Delta t}{M \times \Delta V} \quad (2)$$

$$E = \frac{1}{2} \times C_m \times (\Delta V)^2 \quad (3)$$

$$P_{av} = \frac{E}{\Delta t} \quad (4)$$

$$P_{max} = \frac{(\Delta V)^2}{4M \times R_{ESR}} \quad (5)$$

where C_m (F g^{-1}) is the measured device capacitance, I (A) represents the discharge current, ΔV (V) refers to the potential change within the discharge time Δt (s), M (g) is the total mass of the active material on the two electrodes, E (J g^{-1}) refers to the energy density, P_{av} (W g^{-1}) corresponds to the average power density, P_{max} (W g^{-1}) is the maximum power density, and R_{ESR} (Ω) is the ESR of the electrode.

From the CV curves at different scan rates (Figure 7a), we can see that the N-CNFs-900//N-CNFs-900 device

still maintained the rectangular-shaped cyclic voltammogram even at a high potential scan rate of 200 mV s^{-1}. We calculated the power density and energy density using the data of Figure 7b,c *via* eqs 2−5. The Ragone plot for the electrochemical N-CNFs-900//N-CNFs-900 capacitor in 6.0 mol L^{-1} KOH electrolyte is presented in Figure 7d, showing that the specific energy density for the device is about 7.11 Wh kg^{-1} at a current density of 0.25 A g^{-1}. It is noteworthy to mention that specific energy still is 5.38 Wh kg^{-1} with a high specific power of 15.0 kW kg^{-1} at a current density of 30.0 A g^{-1}, which is higher than that of the commercial carbon supercapacitors (the power density value is 7−8 kW kg^{-1}).[58] Moreover, the value of maximum specific power is 89.57 kW kg^{-1}, which is much higher than that of most commercial aqueous capacitors.[59] The high power density of the electrochemical N-CNFs-900//N-CNFs-900 capacitor is due to the doping of nitrogen (it not only increases the capacitance and electrical conductivity but also improves the wettability of the material in the electrolyte and thus enhances the ion transfer efficiency)[31] and proper pore structure (enhances the kinetics of ion and electron transport in electrodes and at the electrode/electrolyte interface).[60]

Hence, from the above discussions, it can be seen that the N-CNFs-900 electrode material possesses good electrochemical performance. This behavior presumably is associated with the combination effect of the specific surface area, the appreciable N doping amount, the reasonable distribution of pores, and the high conductivity.[3,6,8,24,46,61−63]

CONCLUSION

In summary, we have fabricated a kind of porous nitrogen-doped carbon nanofibers by a facile route, which can be used for the active material of supercapacitor electrodes. Such unique features of composition and structure endow the nitrogen-doped carbon nanofibers with good capacitive performance, that is, with a high electrochemical capacitance (202.0 F g^{-1} at the current density of 1.0 A g^{-1}), good retention capability (81.7% capacitance retention at current densities up to 30 A g^{-1}), large power capability (89.57 kW kg^{-1}), and good cycling stability (3000 cycles). The results demonstrate that the nitrogen-doped carbon nanofibers presented here might be a promising candidate for the electrode material of high-performance supercapacitors. Further engineering of the surface area and composition of this kind of nitrogen-doped carbon nanofibers may provide new possibilities to access high-quality and reliable electrode materials for supercapacitors.

METHODS

All of the chemicals were analytical grade and commercially available from Shanghai Chemical Reagent Co. Ltd. and used as received without further purification.

Preparation Procedures for Carbonaceous Nanofibers. The detailed synthesis procedures of carbonaceous nanofibers (CNFs) were reported elsewhere.[38,40,64,65]

Synthesis of Nitrogen-Doped Carbonaceous Nanofibers. In a typical synthesis, 16 mL of the 8 g L^{-1} CNFs aqueous solution with 0.4 mL of pyrrole was added into 100 mL of deionzed water followed by 5 min of sonication. The mixture was then stirred for 10 min before it was transferred into a beaker. Subsequently, 100 mL of aqueous ammonium persulfate (APS) solution (11.60 mmol L^{-1}) was slowly added into the beaker under continuous stirring at room temperature. After further stirring for 4 h, the product CNFs@polypyrrole (CNFs@Ppy) was separated by filtration, washed with ethanol and water, and dried at 60 °C overnight under vacuum. Finally, the CNFs@Ppy was annealed in a quartz tube under N_2 atmosphere at a flow of 150 cm^3 min^{-1} with a 5 °C min^{-1} heating rate to carbonization temperature (500, 700, 900, and 1100 °C) for 2 h to obtain the nitrogen-doped carbonaceous nanofibers.

Characterizations. Scanning electron microscopy (SEM) was operated on a JEOL JSM-6700F scanning electron microscope operating at 10 kV and a Zeiss Supra 40 high-resolution field-emission scanning electron microscope operating at 5 kV. Transmission electron microscope (TEM) images were obtained from a Hitachi H7650 transmission electron microscope with CCD imaging system on an acceleration voltage of 120 kV. High-resolution transmission electron microscope (HRTEM) images were performed on a JEOL-2010 transmission electron microscope at an acceleration voltage of 200 kV. X-ray diffraction (XRD) data were determined on a Philips X'Pert Pro Super X-ray diffractometer equipped with graphite monochromatized Cu Kα radiation (λ = 1.541841 Å). X-ray photoelectron spectra (XPS) were determined by an X-ray photoelectron spectrometer (ESCALab MKII) with an excitation source of Mg Kα radiation (1253.6 eV). N_2 sorption analysis was conducted on an ASAP 2020 accelerated surface area and porosimetry instrument (Micromeritics), equipped with automated surface area, at 77 K using Barrett−Emmett−Teller (BET) calculations for the surface area. The pore size distribution (PSD) plot was recorded from the adsorption branch of the isotherm based on the Barrett−Joyner−Halenda (BJH) model.

Electrochemical Measurement. All electrochemical experiments were carried out on a CHI 760D electrochemical workstation at room temperature. In a three-electrode system, the test electrode was prepared by loading a slurry consisting of 80 wt % active material, 10 wt % carbon black, and 10 wt % poly(vinylidene fluoride) (PVDF) (in *N*-methylpyrrolidone) on a nickel foam and dried at 80 °C for 1.5 h under vacuum. As-formed electrodes were then pressed at a pressure of 10 MPa and further dried in a vacuum oven at 100 °C overnight. The loading mass of active materials on each current collector was 5.0−6.0 mg, and area was 1.0 cm^2. In the three-electrode system, the sample was used as the test electrode, platinum foil as the counter electrode, Hg/HgO electrode as reference electrode, and 6.0 M KOH aqueous solution as electrolyte. Cyclic voltammetry curves were obtained in the potential range of −1.0−0 V *vs* Hg/HgO by varying the scan rate from 5 to 400 mV s^{-1}. Charge−discharge measurements were carried out galvanostatically at 0.5−30.0 A g^{-1} over a voltage range of −1.0−0 V *vs* Hg/HgO. To construct the electrochemical capacitor N-CNFs-900//N-CNFs-900, the N-CNFs-900 nanocomposite used for the electrode was prepared by mixing 80 wt % N-CNFs-900, 10 wt % carbon black, and 10 wt % PVDF binder, then loaded on the nickel foam and pressed at a pressure of 10 MPa and further dried. The loading mass of N-CNFs-900 in each electrode was 0.0034 g. The two electrodes were separated by a filter paper soaked with electrolyte, then wrapped with parafilm, and at last dipped in the electrolyte solution. The cyclic voltammetry and galvanostatic charge−discharge tests of the electrochemical capacitor (N-CNFs-900//N-CNFs-900) were

performed in a two-electrode cell assembly in the electrolyte of 6.0 M KOH aqueous solution. Electrochemical impedance spectroscopy (EIS) was measured in the frequency range of 10 mHz to 10 kHz at the open circuit voltage with an alternate current amplitude of 5 mV.

Conflict of Interest: The authors declare no competing financial interest.

Acknowledgment. This work is supported by the National Basic Research Program of China (Grant 2010CB934700), the National Natural Science Foundation of China (Grant Nos. 91022032, 21061160492, J1030412), the Chinese Academy of Sciences (Grant KJZD-EW-M01-1), International Science & Technology Cooperation Program of China (Grant 2010DFA41170), and the Principal Investigator Award by the National Synchrotron Radiation Laboratory at the University of Science and Technology of China.

Supporting Information Available: Low-resolution FE-SEM images of CNFs and CNFs@Ppy, low-resolution TEM images of N-CNFs-500, N-CNFs-700, N-CNFs-900, and N-CNFs-1100, XRD patterns of CNFs@Ppy, N-CNFs-500, N-CNFs-700, N-CNFs-900, and N-CNFs-1100, typical charge–discharge curves of CNFs-900, CNFs@Ppy, N-CNFs-500, N-CNFs-700, N-CNFs-900, and N-CNFs-1100 at low and high constant currents, electrochemical impedance spectra collected at open circuit voltage under the influence of an ac voltage of 5 mV (inset shows the magnified spectra). This material is available free of charge *via* the Internet at http://pubs.acs.org.

REFERENCES AND NOTES

1. Dell, R. M.; Rand, D. A. J. Energy Storage - A Key Technology for Global Energy Sustainability. *J. Power Sources* **2001**, *100*, 2–17.
2. Simon, P.; Gogotsi, Y. Materials for Electrochemical Capacitors. *Nat. Mater.* **2008**, *7*, 845–854.
3. Arico, A. S.; Bruce, P.; Scrosati, B.; Tarascon, J. M.; Van Schalkwijk, W. Nanostructured Materials for Advanced Energy Conversion and Storage Devices. *Nat. Mater.* **2005**, *4*, 366–377.
4. Zhang, L. L.; Zhao, X. S. Carbon-Based Materials as Supercapacitor Electrodes. *Chem. Soc. Rev.* **2009**, *38*, 2520–2531.
5. Miller, J. R.; Simon, P. Materials Science: Electrochemical Capacitors for Energy Management. *Science* **2008**, *321*, 651–652.
6. Su, F.; Poh, C. K.; Chen, J. S.; Xu, G.; Wang, D.; Li, Q.; Lin, J.; Lou, X. W. Nitrogen-Containing Microporous Carbon Nanospheres with Improved Capacitive Properties. *Energy Environ. Sci.* **2011**, *4*, 717–724.
7. Zhai, Y.; Dou, Y.; Zhao, D.; Fulvio, P. F.; Mayes, R. T.; Dai, S. Carbon Materials for Chemical Capacitive Energy Storage. *Adv. Mater.* **2011**, *23*, 4828–4850.
8. Zhao, L.; Fan, L. Z.; Zhou, M. Q.; Guan, H.; Qiao, S.; Antonietti, M.; Titirici, M.-M. Nitrogen-Containing Hydrothermal Carbons with Superior Performance in Supercapacitors. *Adv. Mater.* **2010**, *22*, 5202–5206.
9. Andrew, B. R&D Considerations for the Performance and Application of Electrochemical Capacitors. *Electrochim. Acta* **2007**, *53*, 1083–1091.
10. Portet, C.; Yushin, G.; Gogotsi, Y. Electrochemical Performance of Carbon Onions, Nanodiamonds, Carbon Black and Multiwalled Nanotubes in Electrical Double Layer Capacitors. *Carbon* **2007**, *45*, 2511–2518.
11. Pech, D.; Brunet, M.; Durou, H.; Huang, P. H.; Mochalin, V.; Gogotsi, Y.; Taberna, P. L.; Simon, P. Ultrahigh-Power Micrometre-Sized Supercapacitors Based on Onion-like Carbon. *Nat. Nanotechnol.* **2010**, *5*, 651–654.
12. Dai, L.; Chang, D. W.; Baek, J.-B.; Lu, W. Carbon Nanomaterials for Advanced Energy Conversion and Storage. *Small* **2012**, *8*, 1130–1166.
13. Du, F.; Yu, D.; Dai, L.; Ganguli, S.; Varshney, V.; Roy, A. K. Preparation of Tunable 3D Pillared Carbon Nanotube-Graphene Networks for High-Performance Capacitance. *Chem. Mater.* **2011**, *23*, 4810–4816.
14. Choi, H. J.; Jung, S. M.; Seo, J. M.; Chang, D. W.; Dai, L.; Baek, J.-B. Graphene for Energy Conversion and Storage in Fuel Cells and Supercapacitors. *Nano Energy* **2012**, 10.1016/j.nanoen.2012.05.001.
15. Li, L.; Liu, E.; Shen, H.; Yang, Y.; Huang, Z.; Xiang, X.; Tian, Y. Charge Storage Performance of Doped Carbons Prepared from Polyaniline for Supercapacitors. *J. Solid State Electron.* **2011**, *15*, 175–182.
16. Hulicova-Jurcakova, D.; Seredych, M.; Lu, G. Q.; Bandosz, T. J. Combined Effect of Nitrogen- and Oxygen-Containing Functional Groups of Microporous Activated Carbon on Its Electrochemical Performance in Supercapacitors. *Adv. Funct. Mater.* **2009**, *19*, 438–447.
17. Jin, Z.; Yao, J.; Kittrell, C.; Tour, J. M. Large-Scale Growth and Characterizations of Nitrogen-Doped Monolayer Graphene Sheets. *ACS Nano* **2011**, *5*, 4112–4117.
18. Zhao, X.; Wang, A.; Yan, J.; Sun, G.; Sun, L.; Zhang, T. Synthesis and Electrochemical Performance of Heteroatom-Incorporated Ordered Mesoporous Carbons. *Chem. Mater.* **2010**, *22*, 5463–5473.
19. Wang, D.-W.; Li, F.; Chen, Z.-G.; Lu, G. Q.; Cheng, H.-M. Synthesis and Electrochemical Property of Boron-Doped Mesoporous Carbon in Supercapacitor. *Chem. Mater.* **2008**, *20*, 7195–7200.
20. Zheng, Q. B.; Gudarzi, M. M.; Wang, S. J.; Geng, Y.; Li, Z.; Kim, J.-K. Improved Electrical and Optical Characteristics of Transparent Graphene Thin Films Produced by Acid and Doping Treatments. *Carbon* **2011**, *49*, 2905–2916.
21. Worsley, M. A.; Kucheyev, S. O.; Kuntz, J. D.; Olson, T. Y.; Han, T. Y. J.; Hamza, A. V.; Satcher, J. H.; Baumann, T. F. Carbon Scaffolds for Stiff and Highly Conductive Monolithic Oxide-Carbon Nanotube Composites. *Chem. Mater.* **2011**, *23*, 3054–3061.
22. Hulicova-Jurcakova, D.; Puziy, A. M.; Poddubnaya, O. I.; Suárez-García, F.; Tascón, J. M. D.; Lu, G. Q. Highly Stable Performance of Supercapacitors from Phosphorus-Enriched Carbons. *J. Am. Chem. Soc.* **2009**, *131*, 5026–5027.
23. Iyyamperumal, E.; Wang, S.; Dai, L. Vertically Aligned BCN Nanotubes with High Capacitance. *ACS Nano* **2012**, *6*, 5259–5265.
24. Jeong, H. M.; Lee, J. W.; Shin, W. H.; Choi, Y. J.; Shin, H. J.; Kang, J. K.; Choi, J. W. Nitrogen-Doped Graphene for High-Performance Ultracapacitors and the Importance of Nitrogen-Doped Sites at Basal Planes. *Nano Lett.* **2011**, *11*, 2472–2477.
25. Guo, H.; Gao, Q. Boron and Nitrogen Co-doped Porous Carbon and Its Enhanced Properties as Supercapacitor. *J. Power Sources* **2009**, *186*, 551–556.
26. Lee, Y.-H.; Lee, Y.-F.; Chang, K.-H.; Hu, C.-C. Synthesis of N-Doped Carbon Nanosheets from Collagen for Electrochemical Energy Storage/Conversion Systems. *Electrochem. Commun.* **2011**, *13*, 50–53.
27. Hulicova-Jurcakova, D.; Kodama, M.; Shiraishi, S.; Hatori, H.; Zhu, Z. H.; Lu, G. Q. Nitrogen-Enriched Nonporous Carbon Electrodes with Extraordinary Supercapacitance. *Adv. Funct. Mater.* **2009**, *19*, 1800–1809.
28. Kim, N. D.; Kim, W.; Joo, J. B.; Oh, S.; Kim, P.; Kim, Y.; Yi, J. Electrochemical Capacitor Performance of N-Doped Mesoporous Carbons Prepared by Ammoxidation. *J. Power Sources* **2008**, *180*, 671–675.
29. Jurewicz, K.; Babel, K.; Ziolkowski, A.; Wachowska, H. Capacitance Behaviour of the Ammoxidised Coal. *J. Phys. Chem. Solids* **2004**, *65*, 269–273.
30. Cao, B.; Zhang, B.; Jiang, X.; Zhang, Y.; Pan, C. Direct Synthesis of High Concentration N-Doped Coiled Carbon Nanofibers from Amine Flames and Its Electrochemical Properties. *J. Power Sources* **2011**, *196*, 7868–7873.
31. Yang, X.; Wu, D.; Chen, X.; Fu, R. Nitrogen-Enriched Nanocarbons with a 3-D Continuous Mesopore Structure from Polyacrylonitrile for Supercapacitor Application. *J. Phys. Chem. C* **2010**, *114*, 8581–8586.
32. Lee, Y. H.; Lee, Y. F.; Chang, K. H.; Hu, C. C. Synthesis of N-Doped Carbon Nanosheets from Collagen for Electrochemical Energy Storage/Conversion Systems. *Electrochem. Commun.* **2011**, *13*, 50–53.

33. Shrestha, S.; Mustain, W. E. Properties of Nitrogen-Functionalized Ordered Mesoporous Carbon Prepared Using Polypyrrole Precursor. *J. Electrochem. Soc.* **2010**, *157*, B1665–B1672.
34. Konno, H.; Onishi, H.; Yoshizawa, N.; Azumi, K. MgO-Templated Nitrogen-Containing Carbons Derived from Different Organic Compounds for Capacitor Electrodes. *J. Power Sources* **2010**, *195*, 667–673.
35. Fuertes, A. B.; Centeno, T. A. Mesoporous Carbons with Graphitic Structures Fabricated by Using Porous Silica Materials as Templates and Iron-Impregnated Polypyrrole as Precursor. *J. Mater. Chem.* **2005**, *15*, 1079–1083.
36. Ania, C. O.; Khomenko, V.; Raymundo-Piñero, E.; Parra, J. B.; Béguin, F. The Large Electrochemical Capacitance of Microporous Doped Carbon Obtained by Using a Zeolite Template. *Adv. Funct. Mater.* **2007**, *17*, 1828–1836.
37. Lota, G.; Lota, K.; Frackowiak, E. Nanotubes Based Composites Rich in Nitrogen for Supercapacitor Application. *Electrochem. Commun.* **2007**, *9*, 1828–1832.
38. Qian, H. S.; Yu, S. H.; Luo, L. B.; Gong, J. Y.; Fei, L. F.; Liu, X. M. Synthesis of Uniform Te@Carbon-Rich Composite Nanocables with Photoluminescence Properties and Carbonaceous Nanofibers by the Hydrothermal Carbonization of Glucose. *Chem. Mater.* **2006**, *18*, 2102–2108.
39. Hu, B.; Wang, K.; Wu, L. H.; Yu, S. H.; Antonietti, M.; Titirici, M. M. Engineering Carbon Materials from the Hydrothermal Carbonization Process of Biomass. *Adv. Mater.* **2010**, *22*, 813–828.
40. Liang, H. W.; Guan, Q. F.; Chen, L. F.; Zhu, Z.; Zhang, W. J.; Yu, S. H. Macroscopic-Scale Template Synthesis of Robust Carbonaceous Nanofiber Hydrogels and Aerogels and Their Applications. *Angew. Chem., Int. Ed.* **2012**, *51*, 5101–5105.
41. Kapteijn, F.; Moulijn, J. A.; Matzner, S.; Boehm, H. P. The Development of Nitrogen Functionality in Model Chars during Gasification in CO_2 and O_2. *Carbon* **1999**, *37*, 1143–1150.
42. Nishihara, H.; Kwon, T.; Itoi, H.; Yang, Q. H.; Kyotani, T. Enhancement Mechanism of Electrochemical Capacitance in Nitrogen-/Boron-Doped Carbons with Uniform Straight Nanochannels. *Langmuir* **2009**, *25*, 11961–11968.
43. Li, W.; Chen, D.; Li, Z.; Shi, Y.; Wan, Y.; Huang, J.; Yang, J.; Zhao, D.; Jiang, Z. Nitrogen Enriched Mesoporous Carbon Spheres Obtained by a Facile Method and Its Application for Electrochemical Capacitor. *Electrochem. Commun.* **2007**, *9*, 569–573.
44. Tao, Y. S.; Kanoh, H.; Abrams, L.; Kaneko, K. Mesopore-Modified Zeolites: Preparation, Characterization, and Applications. *Chem. Rev.* **2006**, *106*, 896–910.
45. Tao, Y. S.; Tanaka, H.; Ohkubo, T.; Kanoh, H.; Kaneko, K. Pore Structures of ZSM-5 Synthesized in the Mesopore Spaces of a Carbon Aerogel. *Adsorpt. Sci. Technol.* **2003**, *21*, 199–203.
46. Kim, W.; Kang, M. Y.; Joo, J. B.; Kim, N. D.; Song, I. K.; Kim, P.; Yoon, J. R.; Yi, J. Preparation of Ordered Mesoporous Carbon Nanopipes with Controlled Nitrogen Species for Application in Electrical Double-layer Capacitors. *J. Power Sources* **2010**, *195*, 2125–2129.
47. Zhu, T.; Chen, J. S.; Lou, X. W. Shape-Controlled Synthesis of Porous Co_3O_4 Nanostructures for Application in Supercapacitors. *J. Mater. Chem.* **2010**, *20*, 7015–7020.
48. Frackowiak, E.; Lota, G.; Machnikowski, J.; Vix-Guterl, C.; Beguin, F. Optimisation of Supercapacitors Using Carbons with Controlled Nanotexture and Nitrogen Content. *Electrochim. Acta* **2006**, *51*, 2209–2214.
49. Kim, Y. J.; Abe, Y.; Yanagiura, T.; Park, K. C.; Shimizu, M.; Iwazaki, T.; Nakagawa, S.; Endo, M.; Dresselhaus, M. S. Easy Preparation of Nitrogen-Enriched Carbon Materials from Peptides of Silk Fibroins and Their Use To Produce a High Volumetric Energy Density in Supercapacitors. *Carbon* **2007**, *45*, 2116–2125.
50. Beguin, F.; Szostak, K.; Lota, G.; Frackowiak, E. A Self-Supporting Electrode for Supercapacitors Prepared by One-Step Pyrolysis of Carbon Nanotube/Polyacrylonitrile Blends. *Adv. Mater.* **2005**, *17*, 2380–2388.
51. Yang, L.; Cheng, S.; Ding, Y.; Zhu, X.; Wang, Z. L.; Liu, M. Hierarchical Network Architectures of Carbon Fiber Paper Supported Cobalt Oxide Nanonet for High-Capacity Pseudocapacitors. *Nano Lett.* **2012**, *12*, 321–325.
52. Chen, Q. L.; Xue, K. H.; Shen, W.; Tao, F. F.; Yin, S. Y.; Xu, W. Fabrication and Electrochemical Properties of Carbon Nanotube Array Electrode for Supercapacitors. *Electrochim. Acta* **2004**, *49*, 4157–4161.
53. Lu, X.; Wang, G.; Zhai, T.; Yu, M.; Gan, J.; Tong, Y.; Li, Y. Hydrogenated TiO_2 Nanotube Arrays for Supercapacitors. *Nano Lett.* **2012**, *12*, 1690–1696.
54. Chen, Z.; Augustyn, V.; Wen, J.; Zhang, Y. W.; Shen, M. Q.; Dunn, B.; Lu, Y. F. High-Performance Supercapacitors Based on Intertwined CNT/V_2O_5 Nanowire Nanocomposites. *Adv. Mater.* **2011**, *23*, 791–795.
55. Xingyou, L.; Hirata, A.; Fujita, T.; Mingwei, C. Nanoporous Metal/Oxide Hybrid Electrodes for Electrochemical Supercapacitors. *Nat. Nanotechnol.* **2011**, *6*, 232–236.
56. Alshareef, H. N.; Chen, W.; Rakhi, R. B.; Hu, L.; Xie, X.; Cui, Y. High Performance Nanostructured Supercapacitors on a Sponge. *Nano Lett.* **2011**, *11*, 5165–5172.
57. Chen, Z.; Wen, J.; Yan, C.; Rice, L.; Sohn, H.; Shen, M.; Cai, M.; Dunn, B.; Lu, Y. High-Performance Supercapacitors Based on Hierarchically Porous Graphite Particles. *Adv. Energy Mater.* **2011**, *1*, 551–556.
58. Zhu, Y.; Murali, S.; Stoller, M. D.; Ganesh, K. J.; Cai, W.; Ferreira, P. J.; Pirkle, A.; Wallace, R. M.; Cychosz, K. A.; Thommes, M.; Su, D.; Stach, E. A.; Ruoff, R. S. Carbon-Based Supercapacitors Produced by Activation of Graphene. *Science* **2011**, *332*, 1537–1541.
59. Cao, C.-Y.; Guo, W.; Cui, Z.-M.; Song, W.-G.; Cai, W. Microwave-Assisted Gas/Liquid Interfacial Synthesis of Flower-like NiO Hollow Nanosphere Precursors and Their Application as Supercapacitor Electrodes. *J. Mater. Chem.* **2011**, *21*, 3204–3209.
60. Liu, C.; Li, F.; Ma, L. P.; Cheng, H. M. Advanced Materials for Energy Storage. *Adv. Mater.* **2010**, *22*, E28–E62.
61. Ania, C. O.; Khomenko, V.; Raymundo-Pinero, E.; Parra, J. B.; Beguin, F. The Large Electrochemical Capacitance of Microporous Doped Carbon Obtained by Using a Zeolite Template. *Adv. Funct. Mater.* **2007**, *17*, 1828–1836.
62. Aboutalebi, S. H.; Chidembo, A. T.; Salari, M.; Konstantinov, K.; Wexler, D.; Liu, H. K.; Dou, S. X. Comparison of GO, GO/MWCNTs Composite and MWCNTs as Potential Electrode Materials for Supercapacitors. *Energy Environ. Sci.* **2011**, *4*, 1855–1865.
63. Merlet, C.; Rotenberg, B.; Madden, P. A.; Taberna, P.-L.; Simon, P.; Gogotsi, Y.; Salanne, M. On the Molecular Origin of Supercapacitance in Nanoporous Carbon Electrodes. *Nat. Mater.* **2012**, *11*, 306–310.
64. Liang, H. W.; Cao, X.; Zhang, W. J.; Lin, H. T.; Zhou, F.; Chen, L. F.; Yu, S. H. Robust and Highly Efficient Free-Standing Carbonaceous Nanofiber Membranes for Water Purification. *Adv. Funct. Mater.* **2011**, *21*, 3851–3858.
65. Liang, H. W.; Wang, L.; Chen, P. Y.; Lin, H. T.; Chen, L. F.; He, D.; Yu, S. H. Carbonaceous Nanofiber Membranes for Selective Filtration and Separation of Nanoparticles. *Adv. Mater.* **2010**, *22*, 4691–4695.